Surface Science 606 (2012) 1–6

Contents lists available at ScienceDirect

Surface Science

journal homepage: www.elsevier.com/ locate/susc

Surface structure of $In_2O_3(111)$ (1×1) determined by density functional theory calculations and low energy electron diffraction

K. Pussi [a], A. Matilainen [a], V.R. Dhanak [c], A. Walsh [d], R.G. Egdell [b,*], K.H.L. Zhang [b]

[a] Department of Mathematics and Physics, Lappeenranta University of Technology, FIN-53581 Lappeenranta, Finland
[b] Department of Chemistry, University of Oxford, Inorganic Chemistry Laboratory, South Parks Road, Oxford OX1 3QR, UK
[c] Department of Physics, University of Liverpool, Liverpool L69 3BX, UK
[d] Centre for Sustainable Chemical Technologies and Department of Chemistry, University of Bath, Claverton Down, Bath BA2 7AY, UK

ARTICLE INFO

Article history:
Received 4 May 2011
Accepted 19 July 2011
Available online 27 July 2011

Keywords:
Indium oxide
Low energy electron diffraction
Surface structure
Density functional calculations

ABSTRACT

The surface structure of $In_2O_3(111)$ has been investigated by dynamical analysis of low energy electron diffraction data, in conjunction with first principles calculations using density functional theory. The experimental data set consisted of eight independent beams whose intensities were measured for incident energies in the range between 25 eV and 250 eV. In fitting the experimental data it was essential to treat the radii of In and O spheres as variable parameters: following this procedure a final Pendry R factor of 0.31 was obtained. The LEED results are compatible with the calculations and both analyses suggest that the surface structure involves only small vertical relaxations in the outermost of the $\{[O^{2-}]_{12}^{24-}[In^{3+}]_{16}^{48+}[O^{2-}]_{12}^{24-}\}$ quadrupolar units that define the (111) surface. The *ab initio* slab calculations also confirm that lateral relaxations not considered in fitting the experimental data are of very minor importance.

1. Introduction

Sn-doped In_2O_3 is a prototype transparent conducting oxide (TCO) with important applications in heat reflecting mirrors [1], thin film display devices [2] and solar cells [3,4]. Although surface and interface properties are often important to the technological performance of TCOs in these areas, very little is known about the structure of In_2O_3 surfaces. This is in part because of the limited availability of bulk In_2O_3 single crystals. However, there have been important developments in recent years in the epitaxial growth of high quality In_2O_3 single crystals on cubic Y-stabilised ZrO_2 (Y-ZrO_2) substrates [5–13]. This has enabled preparation of ordered (001), (110) and (111) surfaces which have proved amenable to investigation by scanning tunnelling microscopy (STM) [14–16]. The body centred cubic bixbyite structure of In_2O_3 belongs to the space group $Ia\bar{3}$ and has a cubic lattice parameter $a=10.1170$ Å [17]. By contrast the face centred cubic fluorite structure of Y-ZrO_2 belongs to the space group $Fm\bar{3}m$ with lattice parameter $a=5.1423$ Å at the 17% Y doping level found in most commercial substrates [9]. The bixbyite structure is derived from a $2\times2\times2$ superstructure of fluorite but with ¼ of the anion sites vacant. In contrast to the 8-fold coordination of cations within the fluorite structure, the cation sites of bixbyite are all 6-fold coordinate. However two distinct cation sites can be identified: 8b sites with regular octahedral coordination defined by a single In–O bond length of 2.181 Å; and lower symmetry 24d sites where there are three distinct pairs of In–O bond lengths. There is a small mismatch on the order of only 1.6% between $2a$ for Y-doped ZrO_2 (10.2846 Å) and a for In_2O_3, with the epilayer under tensile stress. Moreover the close relationship between the cation arrangements within the two structures ensures that there is minimal chemical mismatch at interfaces between the two. Thus Y-doped ZrO_2 is an ideal substrate for growth of well-ordered thin films of In_2O_3.

In parent fluorite-type oxides such as Y-ZrO_2 [18,19] and UO_2 [20], the sequence of energies for the low index surfaces follows the order $\gamma(001)>\gamma(110)>\gamma(111)$ [21]. The high energy (001) surface is a polar Tasker type III surface with alternating cation and anion containing planes [22] whilst the intermediate (110) surface is Tasker type I with charge neutral layers. The lowest energy (111) surface is Tasker type II and is based on a sequence of anion and cation layers which may be grouped into charge neutral quadrupolar layers. The sequence of surface energies for bixbyite In_2O_3 is the same as for fluorite-like oxides, although there are small displacements in the ionic positions so that successive layers of ions are not rigorously coplanar as in fluorite itself but are characterised by a straddle of positions above and below the idealised fluorite positions [21]. Using the idealised layer description, the lowest energy (111) surface structure is based on repeating quadrupolar units with overall stoichiometry $\{[O^{2-}]_{12}^{24-}[In^{3+}]_{16}^{48+}[O^{2-}]_{12}^{24-}\}$: there are three of these repeat units before registry is restored in lateral positions in the fourth quadrupolar layer. It is possible to grow continuous (111) oriented epitaxial thin films with reasonably flat surfaces under a range of conditions, whereas in growth on (110) or (001) oriented substrates there is a propensity

* Corresponding author. Tel.: +44 1 865 2 85157.
E-mail address: Russell.egdell@chem.ox.ac.uk (R.G. Egdell).

0039-6028/$ – see front matter © 2011 Elsevier B.V. All rights reserved.
doi:10.1016/j.susc.2011.07.014

toward development of islands with low energy (111) side facets [5,9,21,23]. Thus as a first step toward systematic investigation of the structures of low index In_2O_3 surfaces, a study of In_2O_3(111) is an obvious starting point.

We present here a determination of the structure of the (1×1) reconstruction of Sn-In_2O_3(111) by analysis of intensity/voltage (I/V) curves in low energy electron diffraction (LEED). In_2O_3 has 80 atoms in the unit cell and fitting the LEED data to an experimental structure is not trivial. However we have reached an acceptable Pendry R factor of 0.31. It transpires that the experimental structure is derived from a simple bulk termination with relaxations normal to the surface which cause a small reduction in the spacings between the In and O atoms in the outer quadrupolar layer. Reasonable agreement is found between the experimental surface structure and that derived from *ab initio* density functional theory calculations, which suggest that both vertical and lateral relaxations are small.

2. Experimental section

To minimise the effects of sample charging, LEED studies were conducted on lightly n-type doped In_2O_3 (with Sn as the dopant) rather than nominally undoped material. It has also been shown that Sn doping leads to improvement in the smoothness of In_2O_3 thin films [24]. Epitaxial thin films of 3% Sn-doped In_2O_3 were grown on 1 cm×1 cm Y-stabilized ZrO_2(111) substrates in an ultrahigh vacuum oxide MBE system (SVT, USA) with a base pressure of 5×10^{-10} mbar. This incorporated a hot lip indium Knudsen cell, a conventional Sn Knudsen cell and a radio frequency (RF) plasma oxygen atom source operated at 200 mW RF power with an oxygen background pressure of 3×10^{-5} mbar. Substrates were heated radiatively using a graphite filament. The nominal growth rate was 0.035 nm s^{-1}, as calibrated from the film thickness derived from HRTEM measurements. The Y-ZrO_2 substrates were cleaned by exposure to the oxygen atom beam at a nominal substrate temperature of 900 °C. Films were then grown to a thickness of 210 nm at a substrate temperature of 700 °C. *In situ* display LEED was carried out in an analysis chamber connected to the growth chamber, which revealed a well ordered (1×1) reconstruction. This reconstruction was easily regenerated in a second ultra high vacuum (UHV) system. The *ex situ* experiments were conducted in a standard UHV surface science chamber containing a PSP Vacuum Technology electron energy analyser, dual anode X-ray source, rear view LEED optics from OCI Vacuum Microengineering and an Omicron scanning tunnelling microscopy module (STM1) operating at room temperature. The base pressure of the system was less than 2×10^{-10} mbar, with hydrogen as the main residual gas in the chamber. The Sn doped In_2O_3 samples were cleaned by repeated cycles of bombardment with 500 eV argon ions followed by annealing at 500 °C for 30 min in ultrahigh vacuum (UHV). The cleanliness of the final surface was confirmed by x-ray photoelectron spectroscopy (XPS), where no C 1 s signal could be observed. There was no evidence of pronounced surface segregation of Sn and from the observed ratio of intensities between In 3*d* and Sn 3*d* core lines (Fig. 1) it was estimated that the Sn/In ratio in the near surface probed by XPS was very close to the nominal bulk value of 0.03. The occupation of some In sites by Sn introduces extra complexity into an already complex problem, but it was impossible to obtain LEED data from undoped samples of a quality comparable to that from doped samples.

Large area STM images were obtained in constant-current mode with a chemically etched tungsten tip at room temperature. These revealed that the prepared surfaces contained large flat terrace areas separated by steps of a height $a/2\sqrt{3}=2.9$ Å, corresponding to the separation between successive In layers (Fig. 2).

The surfaces gave sharp (1×1) LEED patterns with a low background (Fig. 3). The intensities of the diffraction spots as a function of the energy of the incident electrons (LEED I–V spectra) were measured at normal incidence of the primary beam. The spectra were background subtracted and normalised with respect to the primary beam current. The intensities of the symmetrically equivalent spots were averaged in order to reduce experimental noise. The data set that was gathered at 300 K consisted of 8 beams, ranging in energy from 20 eV to a maximum of 250 eV. The cumulative energy range was 1270 eV. The useful energy range was limited by two factors. Firstly owing to the large lateral size of the surface unit cell, low order spots converged into the electron gun at fairly low kinetic energies. Secondly higher order spots rapidly faded into the background for kinetic energies much in excess of 200 eV, thus imposing further limitations on the data range.

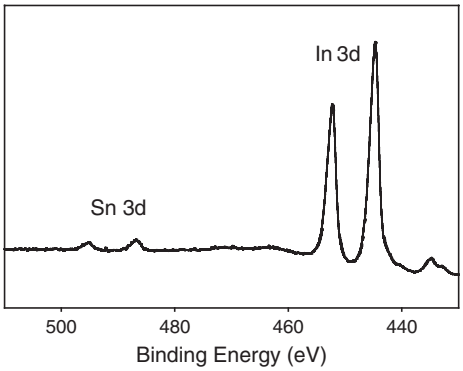

Fig. 1. Core level XPS of Sn-doped In_2O_3(111) film in the In 3*d* and Sn 3*d* core level region measured *in situ* in the LEED system.

3. Density functional theory calculations on In_2O_3(111)

The relaxed surface structure of In_2O_3(111) was calculated using density functional theory (DFT), within the generalized gradient approximation using a Perdew–Burke–Ehrnzerhof (PBE) functional [25], as implemented in the VASP package [26,27]. The plane-wave kinetic energy threshold (500 eV) and *k*-point density (4×4×4) were both well-converged for the bulk system. Starting from the relaxed bulk bixbyite lattice ($a=10.293$ Å), 2D surface models were constructed using a periodic arrangement of slabs, separated with a 20 Å vacuum region. Convergence of the surface energy γ with respect to slab thickness resulted in a model containing 48 formula units (i.e. 6 quadrupolar layers) for the (111) surface. Ions in the top two quadrupolar units were allowed

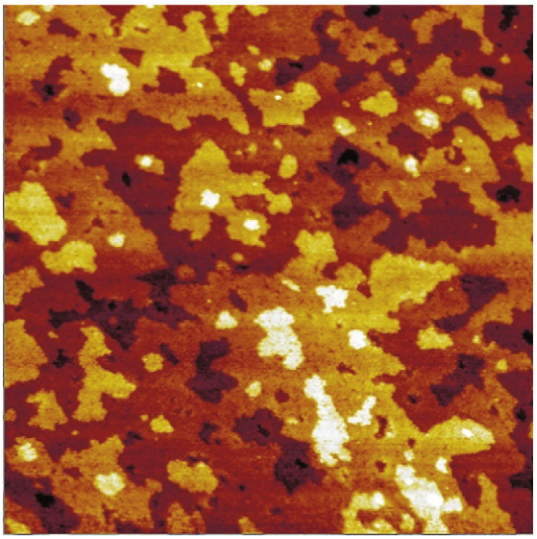

Fig. 2. (Colour online) STM image (200 nm×200 nm) of Sn-In_2O_3 epilayer measured after completion of LEED I/V experiments showing atomic scale steps of height 0.291 nm, corresponding to $a/2\sqrt{3}$. $V_{sample}=+1.5$ V; $I_{current}=0.1$ nA.

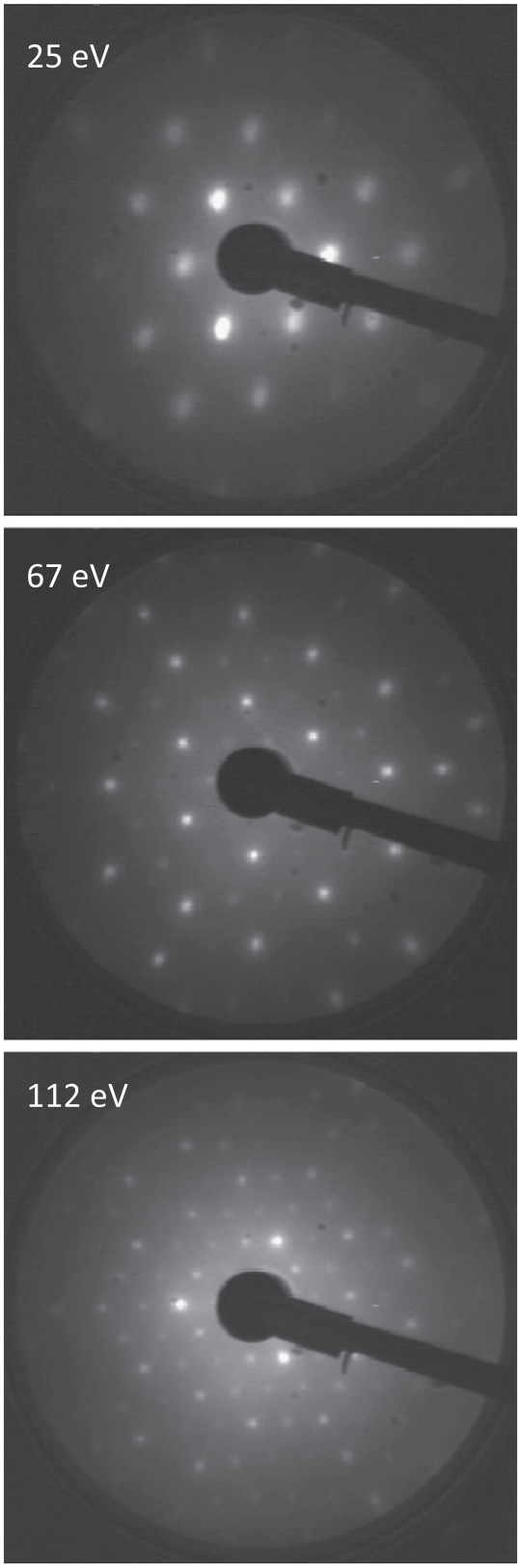

Fig. 3. LEED patterns from Sn-In_2O_3(111) measured at the voltage indicated.

to relax, while all other layers were held at their bulk lattice positions. Simulated annealing was performed to assess the stability of the resulting structures at 750 K and no further relaxations or reconstructions were found to occur. Indeed from a comparison of the low index terminations at the same level of theory, the (111) surface was found to be thermodynamically stable [28]. Lateral relaxations were found to be very small, especially in the second quadrupolar layer where all lateral movements were less than 0.06 Å: in the outer O and In layers most lateral relaxations were less than 0.10 Å, with maximum values of 0.17 Å for O and In with reduced coordination environments. Vertical relaxations were also small, as will be discussed below. The full set of atomic coordinates in 3 column file format are provided as supplementary information in the files DFT-BULKCUTSURFACE.xyz and DFT-RELAXEDSURFACE.xyz for bulk cut and relaxed surfaces respectively.

4. Analysis of LEED data

The dynamical LEED calculations were performed using the Tensor-LEED program [29]. The relativistic phase shifts were calculated using the phase shift program [30] that is packaged with Tensor-LEED. The agreement between the theory and the experiment was tested using the Pendry R-factor and the error bars quoted are calculated using the Pendry RR-function [31]. Four different sets of phase shifts were used: two for oxygen and two for indium. At the beginning of the analysis the Debye temperatures were set to 1000 K for both O and In. The l_{max} value was set to 8 and the imaginary part of inner potential was set to −5.0 eV. These values were optimised in the final stages of the analysis. The real part of the inner potential is independent of energy and was allowed to relax as is normal in LEED analysis.

It is customary to use different Debye temperatures for surface and bulk atoms in LEED analysis. This does not usually have any effect on the geometry of the model but it usually makes the agreement (R-factor) better. In the current work the O atoms in the outermost layer and the In atoms in the top quadrupole were given a different Debye temperature to the values for bulk O and bulk In. The starting values for the Debye temperatures were chosen by "trial and error" starting from the tabulated value of 108 K for In and 500 K for O. Surprisingly high Debye temperature values were favoured for both O and In (1000 K). After refinement of the atomic positions, the Debye temperature were optimized in a final refinement cycle (with fixed atomic positions) to 400 K and 700 K for the "surface" and bulk In respectively and to 1100 K and 1500 K for the surface and bulk O.

The calculation of phase shifts for metal oxides is addressed in detail in the paper of Nascimento et al. [32]. These authors review the methods that have been used previously and also prescribe a technique for calculating the phase shifts for metal oxides. Because of the charge transfer between the oxygen and metal atoms, the calculation of phase shifts is less straightforward than is usual. Instead of using empirical muffin tin radii for neutral atoms as is usually the case, one must take account must be taken of the fact that the fact that the In cations have *smaller* radii than neutral In and the oxide ions will have *larger* radii than the neutral O atom. However there is substantial covalency in In_2O_3 so that *a priori* it may be anticipated that the values will be quite close to those for the neutral atoms. In this paper we have chosen to make arbitrary adjustments to the radii for In and O in the phase shift calculation, until the best fit was reached. The final values of the radii were 1.57 Å for In (bulk value 1.625 Å) and 0.65 Å for O (bulk value 0.60 Å).

Nascimento et al. [32] also discussed the use of energy dependent imaginary and real parts of the inner potential. In the current study the energy dependence of the real and imaginary components of the inner potential was also considered, but in our case it did not have any effect on the R factor. This is probably due the fact that the energy range of our study is quite small (20–250 eV) and the changes in the inner potential in this range are also likely to be small. Also our data did not have many peaks. Ignoring the energy dependence of inner potential could cause systematic errors if one had a data set with a large energy range and many peaks in the data (because the Pendry R-factor is most sensitive to the peak positions).

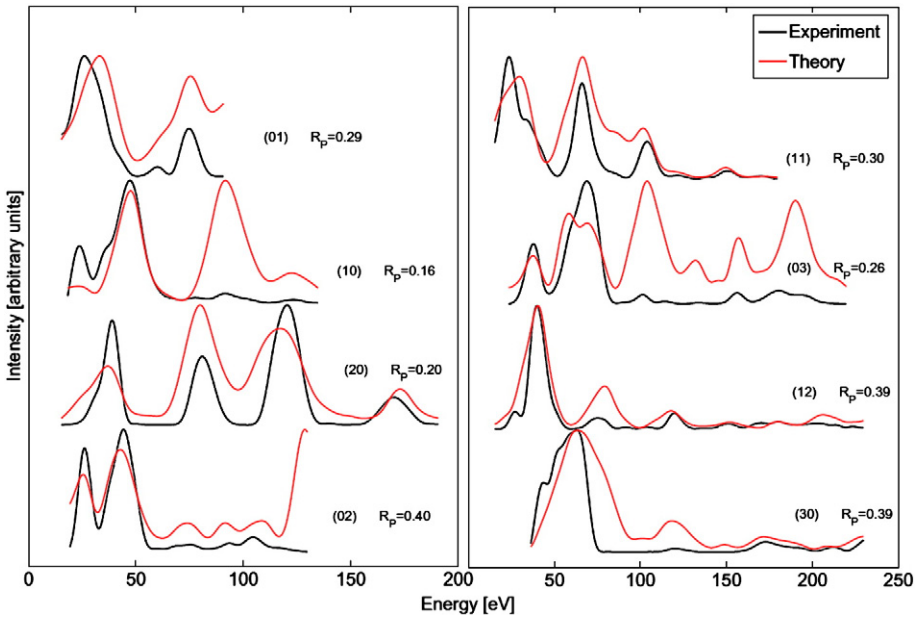

Fig. 4. (Colour online) Experimental LEED I/V data for the 8 independent beams used to determine the surface structure of Sn-In_2O_3(111) along with I/V curves computed for the refined structure. The Pendry R-factors for the individual beams are indicated in the figure.

The geometrical parameters are optimized only in the vertical (z) direction, because normal incidence LEED is not very sensitive to the lateral parameters and our data set was limited in range. However, as discussed above, the DFT studies suggest that lateral relaxations are in general very small indeed. The ions in the top two quadrupolar layers were allowed to relax normal to the surface and the deeper layers were kept fixed, as in the DFT calculations. Although 80 atoms were therefore allowed to relax, symmetry constraints dictated that only 28 positional parameters were refined, along with the real part of the inner potential. This corresponds to 1270/29 eV = 44 eV of raw data per parameter. All parameters were refined simultaneously, starting from an experimental bulk cut structure. Since the DFT calculations had not suggested alternative low energy structures, no alternative structures were refined. However in some preliminary investigations the structural refinement was launched from a starting point where the lattice was expanded by about 8% in the z direction. This structure refined back toward essentially the same the bulk cut structure as found in our final analysis.

For indium atoms the final error bars are between 0.03 Å and 0.06 Å in the outer quadrupolar layer and between 0.07 Å and 0.14 Å in the next layer. The error bars on the oxygen positions are larger and increase with depth below the surface from 0.07 Å and 0.10 Å in the outermost layer through ranges of 0.14 Å - 0.20 Å, 0.20 Å - 0.30 Å and 0.30 Å - 0.30 Å in the next three layers. For some oxygen ions no error bars could be defined, because the R-factor curve was flat around the oxygen position. The final Pendry R-factor is 0.31. Fig. 4 shows the comparison between the best fit I/V curves and the experimental data for the 8 independent beams that were studied. The intensities of calculated features in the I/V curves are in some cases rather poor, but it needs to be remembered that the Pendry R factor deliberately downgrades the importance of fitting peak intensities and emphasises fitting peak positions.

The full set of refined coordinates in .xyz format readable by Crystal Maker software are provided as supplementary information in the file In2O3(111)LEED.xyz

5. Discussion

The Pendry R factor (R_P) of 0.31 derived from the fit to experimental data in the present work is comparable to values reported in recent surface structure determinations for oxides by LEED I/V analysis e.g. $Ca_{1.5}Sr_{0.5}RuO_4$ $R_P = 0.28$ [32]; TiO_2(110) (1×1) $R_P = 0.29$ [33] recently improved to $R_P = 0.23$ [34]; Fe_3O_4(001) ($\sqrt{2}\times\sqrt{2}$) R45° $R_P = 0.34$ [35]; and CoO(001) on Ag(001) $R_P = 0.27$ [36]. It may be noted that in the current study 29 parameters were refined, so that the complexity of the problem is comparable to that for Fe_3O_4(001) ($\sqrt{2}\times\sqrt{2}$) where 53 structural parameters were refined. The final R factors in these two structural determinations are very similar. Of course much lower R factors are typically obtained for simple metal or semiconductor surfaces.

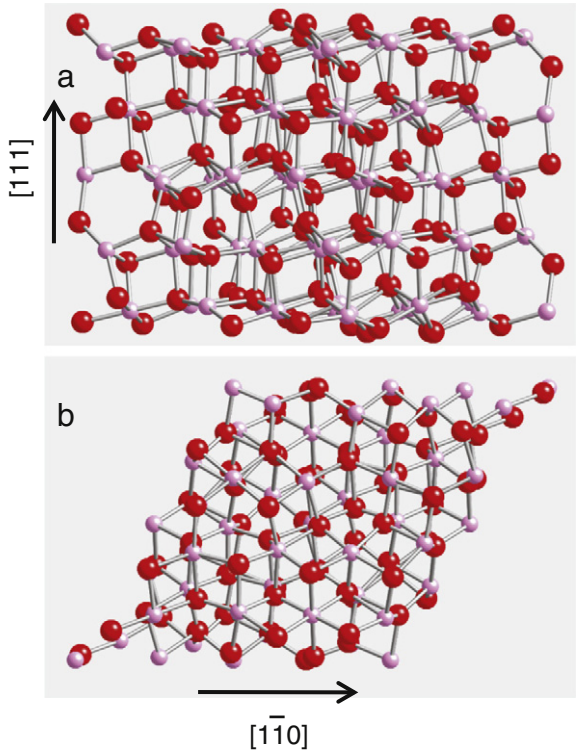

Fig. 5. (Colour online) The relaxed surface structure of In_2O_3(111) derived from LEED. (a) Shows a side view with the [111] direction running vertically, while (b) shows a top view down the the [111] axis. Smaller paler spheres (pink online) are In and larger darker spheres (red online) are O.

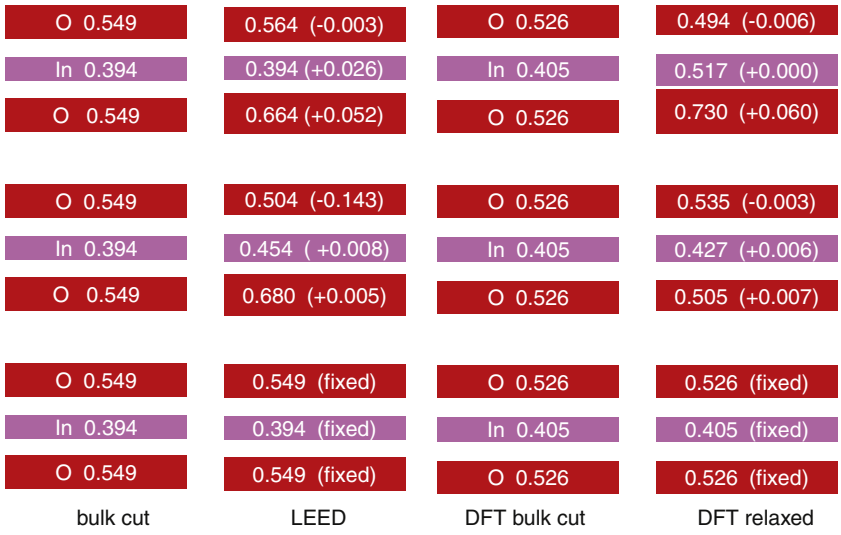

Fig. 6. (Colour online) Schematic representation of the structure for $In_2O_3(111)$ derived from truncation of the bulk structure and from analysis of LEED I/V data. Comparative diagrams for a bulk cut DFT structure and a relaxed DFT structure are also shown. Owing to the complexity of the structures individual atomic positions are not shown but the spread of atomic positions within components of the quadrupolar layers that are characteristic of the (111) surface are represented by the width of the horizontal stripes. The numbers inside the stripes give the staddle of atomic positions within a layer (in Å), while the figures in parentheses for the LEED and relaxed DFT structures give the average vertical relaxation of the atoms within a given layer (also in Å).

The structure derived from the LEED experiments is shown in Fig. 5. The experimental surface structure depicted is very close to the bulk truncated structure although there are very small vertical relaxations with the following ranges in successive ionic layers: $O_{1(outer)}$ −0.18 Å to +0.19 Å; In_1 −0.07 Å to +0.13 Å; $O_{1(inner)}$ −0.04 Å to +0.21 Å; $O_{2(outer)}$ −0.37 Å to +0.11 Å; In_2 −0.03 Å to +0.11 Å; $O_{2(inner)}$ −0.09 Å to +0.17 Å. In most cases these relaxations are comparable with the error bars. Due to the minor redistributions of the In and O positions within the relevant atomic layers the straddle in ion positions within a single ionic layer close to the surface is slightly different to that in the bulk. This is particularly apparent in the "inner" O layer of the first quadrupole. There is also a small contraction in the distances between the ions in the outermost $\{[O^{2-}]_{12}^{24-}[In^{3+}]_{16}^{48+}[O^{2-}]_{12}^{24-}\}$ quadrupolar unit by a net inward relaxation of the outermost $[O^{2-}]_{12}^{24-}$ layer coupled outward relaxation of the first $[In^{3+}]_{16}^{48+}$ layer and even more pronounced outward relaxation of the next O layer. A schematic of the experimentally determined structure is shown in Fig. 6 alongside a similar schematic for the bulk truncated structure. This diagram represents the successive O–In–O–O–In–O ionic layers in terms of a series of horizontal stripes.

The widths of the stripes in this figure represent the straddle in the distribution of atomic positions within the layers, whilst the numbers within the stripes of the LEED structure indicate the average relaxation in atomic positions within a given stripe. For comparison the figure also includes an analogous schematic representation of the bulk cut and relaxed surface structures derived from DFT calculations. In general there is good agreement between the magnitudes and directions of the average relaxations as derived from LEED and DFT calculations.

The very small relaxations found in the present study are comparable to those found in a LEED study of the (111) surfaces of the ionic fluorite compounds CaF_2 and BaF_2 [37]. Here the outer fluoride ions were found to have inward relaxations of 0.03 Å and 0.12 Å respectively, but the inward relaxation of the outermost cation layer was only 0.01 Å in each case. Similarly for $UO_2(111)$, potential based models [38] suggest an inward relaxation of 0.11 Å for the outer oxygen layer but an *outward* relaxation of 0.03 Å for the first uranium layer.

6. Conclusions

Using a combination of first-principles electronic structure calculations and low energy electron diffraction on single-crystal thin films, the surface structure of $In_2O_3(111)$ has been determined. Our results emphasise the benefit of a multi-technique approach to resolving surface structure. The surface structure involves small vertical relaxations in the outer two charge neutral units that define the (111) surface. The same features are expected for other materials adopting the bixbyite crystal structure.

Acknowledgements

K.P. and A.M. would like to thank Academy of Finland for funding and CSC IT Center for Sciences Ltd. for provision of computational resources. K.H.L.Z. is grateful to the University of Oxford for the award of a Clarendon Scholarship. The Oxford Oxide MBE project was funded by EPSRC grant GR/94148. The work of A.W. has been supported by membership of the UK's HPC Materials Chemistry Consortium, which is funded by EPSRC grant EP/F067496.

Appendix A. Supplementary data

Supplementary data to this article can be found online at doi:10.1016/j.susc.2011.07.014.

References

[1] I. Hamberg, C.G. Granqvist, J. Appl. Phys. 60 (1986) R123.
[2] D.S. Ginley, H. Hosono, D.C. Paine (Eds.), Handbook of Transparent Conductors, Springer, New York, 2010.
[3] C.G. Granqvist, A. Hultaker, Thin Solid Films 411 (2002) 1.
[4] C.G. Granqvist, Int. J. Nanotechnol. 6 (2009) 785.
[5] O. Bierwagen, M.E. White, M.Y. Tsai, J.S. Speck, Appl. Phys. Lett. 95 (2009) 262105.
[6] O. Bierwagen, J.S. Speck, Appl. Phys. Lett. 97 (2010) 072103.
[7] O. Bierwagen, J.S. Speck, J. Appl. Phys. 107 (2010) 113159.
[8] A. Bourlange, D.J. Payne, R.G. Egdell, J.S. Foord, P.P. Edwards, M.O. Jones, A. Schertel, P.J. Dobson, J.L. Hutchison, Appl. Phys. Lett. 92 (2008) 092117.
[9] A. Bourlange, D.J. Payne, R.G. Palgrave, J.S. Foord, R.G. Egdell, R.M.J. Jacobs, A. Schertel, J.L. Hutchison, P.J. Dobson, Thin Solid Films 517 (2009) 4286.
[10] P.D.C. King, T.D. Veal, F. Fuchs, C.Y. Wang, D.J. Payne, A. Bourlange, H.L. Zhang, G.R. Bell, V. Cimalla, O. Ambacher, R.G. Egdell, F. Bechstedt, C.F. McConville, Phys. Rev. B 79 (2009) 205211.
[11] H. Ohta, M. Orita, M. Hirano, H. Tanji, H. Kawazoe, H. Hosono, Appl. Phys. Lett. 76 (2000) 2740.
[12] H. Ohta, M. Orita, M. Hirano, H. Hosono, J. Appl. Phys. 91 (2002) 3547.
[13] T. Koida, M. Kondo, J. Appl. Phys. 99 (2006) 123703.
[14] E.H. Morales, Y.B. He, M. Vinnichenko, B. Delley, U. Diebold, New J. Phys. 10 (2008) 125030.
[15] E.H. Morales, U. Diebold, Appl. Phys. Lett. 95 (2009) 253105.

[16] K.H.L. Zhang, D.J. Payne, R.G. Palgrave, V.K. Lazarov, W. Chen, A.T.S. Wee, C.F. McConville, P.D.C. King, T.D. Veal, G. Panaccione, P. Lacovig, R.G. Egdell, Chem. Mater. 21 (2009) 4353.
[17] M. Marezio, Acta Crystallogr. 20 (1966) 723.
[18] G. Ballabio, M. Bernasconi, F. Pietrucci, S. Serra, Phys. Rev. B 70 (2004) 075417.
[19] F. Lallet, N. Olivi-Tran, L.J. Lewis, Phys. Rev. B 79 (2009) 035413.
[20] F.N. Skomurski, R.C. Ewing, A.L. Rohl, J.D. Gale, U. Becker, Am. Mineral. 91 (2006) 1761.
[21] K.H.L. Zhang, A. Walsh, C.R.A. Catlow, V.K. Lazarov, R.G. Egdell, Nano Lett. 10 (2010) 3740.
[22] P.W. Tasker, J. Phys. C-Solid State Physics 12 (1979) 4977.
[23] A. Bourlange, D.J. Payne, R.M.J. Jacobs, R.G. Egdell, J.S. Foord, A. Schertel, P.J. Dobson, J.L. Hutchison, Chem. Mater. 20 (2008) 4551.
[24] A. Bourlange, D.J. Payne, R.G. Palgrave, H. Zhang, J.S. Foord, R.G. Egdell, R.M.J. Jacobs, T.D. Veal, P.D.C. King, C.F. McConville, J. Appl. Phys. 106 (2009) 013703.
[25] J.P. Perdew, K. Burke, M. Ernzerhof, Phys. Rev. Lett. 77 (1996) 3865.
[26] G. Kresse, J. Furthmuller, Phys. Rev. B 54 (1996) 11169.
[27] G. Kresse, D. Joubert, Phys. Rev. B 59 (1999) 1758.
[28] A. Walsh, C.R.A. Catlow, J. Mat. Chem. 20 (2010) 10438.
[29] M.A. Vanhove, W. Moritz, H. Over, P.J. Rous, A. Wander, A. Barbieri, N. Materer, U. Starke, G.A. Somorjai, Surf. Sci. Reports 19 (1993) 191.
[30] A. Barbieri, M.A. Vanhove, unpublished.
[31] J.B. Pendry, J. Phys. C-Solid State Phys. 13 (1980) 937.
[32] V.B. Nascimento, R.G. Moore, J. Rundgren, J.D. Zhang, L. Cai, R. Jin, D.G. Mandrus, E.W. Plummer, Phys. Rev. B 75 (2007) 035408.
[33] R. Lindsay, A. Wander, A. Ernst, B. Montanari, G. Thornton, N.M. Harrison, Phys. Rev. Lett. 94 (2005) 153404.
[34] W. Busayaporn, X. Torrelles, A. Wander, S. Tomic, A. Ernst, B. Montanari, N.M. Harrison, O. Bikondoa, I. Joumard, J. Zegenhagen, G. Cabailh, G. Thornton, R. Lindsay, Phys. Rev. B 81 (2010) 1299.
[35] R. Pentcheva, W. Moritz, J. Rundgren, S. Frank, D. Schrupp, M. Scheffler, Surf. Sci. 602 (2008) 1299.
[36] K.M. Schindler, J. Wang, A. Chasse, H. Neddermeyer, W. Widdra, Surf. Sci. 603 (2009) 2658.
[37] J. Vogt, J. Henning, H. Weiss, Surf. Sci. 578 (2005) 57.
[38] P.W. Tasker, Surf. Sci. 87 (1979) 315.